Nephrol Dial Transplant (2018) 33: 1514–1525
doi: 10.1093/ndt/gfy057
Advance Access publication 9 April 2018

ndt
Nephrology Dialysis Transplantation

ORIGINAL ARTICLE

Inverse correlation between vascular endothelial growth factor back-filtration and capillary filtration pressures

Christoph Kuppe[1], Wilko Rohlfs[2], Martin Grepl[3], Kevin Schulte[1,4], Delma Veron[5], Marlies Elger[6], Silja Kerstin Sanden[1], Turgay Saritas[1], Johanna Andrae[7], Christer Betsholtz[7], Christian Trautwein[8], Ralf Hausmann[9], Susan Quaggin[10], Sebastian Bachmann[11], Wilhelm Kriz[6], Alda Tufro[5], Jürgen Floege[1] and Marcus J. Moeller[1,12,13]

[1]Division of Nephrology and Immunology, RWTH Aachen University, Aachen, Germany, [2]Institute of Heat and Mass Transfer, RWTH Aachen University, Aachen, Germany, [3]Numerical Mathematics, Faculty for Mathematics, Informatics and Natural Sciences, RWTH Aachen University, Aachen, Germany, [4]Department of Nephrology, University of Kiel, Kiel, Germany, [5]Department of Pediatrics, Yale University School of Medicine, New Haven, CT, USA, [6]Department of Anatomy and Developmental Biology, Medical Faculty Mannheim, University of Heidelberg, Mannheim, Germany, [7]Department of Immunology, Genetics and Pathology, Uppsala University, Rudbeck Laboratory, Uppsala, Sweden, [8]Division of Gastroenterology and Endocrinology, RWTH Aachen University Hospital, Aachen, Germany, [9]Institute of Molecular Pharmacology, RWTH Aachen University Hospital, Aachen, Germany, [10]Division of Medicine-Nephrology, Feinberg Cardiovascular Research Institute, Northwestern University Feinberg School of Medicine, Chicago, IL, USA, [11]Department of Anatomy, Charité Universitätsmedizin, Berlin, Germany, [12]Interdisciplinary Centre for Clinical Research (IZKF Aachen), RWTH Aachen University Hospital, Aachen, Germany and [13]Heisenberg Chair for Preventive and Translational Nephrology, Division of Nephrology, RWTH Aachen University, Aachen, Germany

Correspondence and offprint requests to: Marcus J. Moeller; E-mail: mmoeller@ukaachen.de

ABSTRACT

Background. Vascular endothelial growth factor A (VEGF) is an essential growth factor during glomerular development and postnatal homeostasis. VEGF is secreted in high amounts by podocytes into the primary urine, back-filtered across the glomerular capillary wall to act on endothelial cells. So far it has been assumed that VEGF back-filtration is driven at a constant rate exclusively by diffusion.

Methods. In the present work, glomerular VEGF back-filtration was investigated *in vivo* using a novel extended model based on endothelial fenestrations as surrogate marker for local VEGF concentrations. Single nephron glomerular filtration rate (SNGFR) and/or local filtration flux were manipulated by partial renal mass ablation, tubular ablation, and in transgenic mouse models of systemic or podocytic VEGF overexpression or reduction.

Results. Our study shows positive correlations between VEGF back-filtration and SNGFR as well as effective filtration rate under physiological conditions along individual glomerular capillaries in rodents and humans.

Conclusion. Our results suggest that an additional force drives VEGF back-filtration, potentially regulated by SNGFR.

Keywords: endothelium, filtration, GFR, glomerular hypertrophy, VEGF, streaming potential

INTRODUCTION

In the renal glomerulus, vascular endothelial growth factor A (VEGF) is derived almost exclusively from the visceral epithelium (termed 'podocytes', Supplementary data, Figure S1A) and ablation of VEGF secretion specifically in podocytes results in loss of glomerular endothelial cells [1]. The major VEGF receptor VEGF-R2 (flk-1/KDR) is expressed on endothelial cells [2] and podocytes [3]. Thus, VEGF is likely to be back-filtered against the bulk current of the glomerular filtrate towards the capillary lumen. It has been proposed that about a third of podocyte-derived VEGF reaches the glomerular endothelial cells via diffusion [4].

Multiple studies in animals and humans show that glomerular hypertrophy marks the risk of kidney disease [5–8]. However, the mechanism linking renal plasma flow, glomerular filtration rate (GFR) and glomerular hypertrophy remains unclear [5–8]. Rapid increases in GFR are mediated, at least in part, by volume retention and vasoactive mediators such as nitric oxide and kallikrein [9]. Classical diseases of Western society (i.e. obesity, metabolic syndrome, hypertension, diabetes, and high-protein diets) are associated with glomerular hyperfiltration and hypertrophy [10, 11], which drive progression to end-stage renal disease. Therefore, unravelling the mechanism of glomerular hypertrophy is of paramount importance.

It is well-established that VEGF induces neoangiogenesis in peripheral capillary beds [12]. Within the glomerulus of the kidney, increased levels of VEGF induce glomerular hypertrophy (i.e. growth of glomerular capillaries, Supplementary data, Figure S1A, right) [13–15]. Vice versa, decreased VEGF levels result in significantly smaller glomeruli (hypoplasia) [16], demonstrating that tightly regulated levels of VEGF are necessary to maintain a normal glomerular phenotype.

The present study analyses endothelial morphology as surrogate marker for VEGF back-filtration in the renal glomerulus. We find an unexpected positive correlation between effective filtration pressures [and single-nephron glomerular filtration rate (SNGFR)] with VEGF back-filtration. Mathematical modelling suggests electrical effects as a candidate force to drive this relationship.

MATERIALS AND METHODS

Animal experimental procedures were performed according to German and European Legislation and approved by the local authorities (see cited references). Animals were housed under standard specific pathogen-free (SPF)-free conditions. Pax8-Cre/beta-catenin$^{fl/fl}$ knock-out mice, Pod-rtTA/Tet-O-siVEGF (5 weeks old, 7 days of Dox) and Pod-rtTA/$(tetO)_7$VEGF (8 weeks old) were described in references [13], [16] and [17], respectively. When using transgenic mice, exclusively non-transgenic or single-transgenic littermates were used.

The Pax8-rtTA/$(tetO)_7$VEGF (mixed genetic background, 8 weeks old) animals received doxycycline hydrochloride via the drinking water *ad libitum* for a total of 14 or 30 days (5% sucrose, 1 mg doxycycline/mL, protected from light), which was exchanged every 2 days.

For '5/6 nephrectomy', C57/Bl6 mice aged 8 weeks were anaesthetized with ketamine-xylazine (100 mg/mL ketamine and 20 mg/mL xylazine in normal saline 0, 9%; 0, 1 mL/10 g of bodyweight) and after shaving a laparotomy was made. The right kidney was removed and the upper and lower poles of the left kidney (two-thirds) were excised and Gelastypt (Sanofi-Aventis, Frankfurt, Germany) was used to stop bleeding. GFR measurements were performed as described [18] by injecting dialysed FITC-inulin (3.74 µL/g body weight) retroorbitally under brief isoflurane anaesthesia. Approximately 20 µL of blood were collected via the saphenous vein at 3, 7, 15, 35 and 55 min post-injection (10 µL of plasma). Using semi-quantitative RT-PCR glomeruli were isolated on Day 2 and Day 5 after 5/6UNx using magnetic beads (verified >90% purity). Total ribonucleic acid (RNA) was isolated using the RNeasy Mini Kit (Qiagen, Hilden, Germany). Quantification of the RNA content and sample purity, complementary deoxyribonucleic acid (cDNA) synthesis and real-time quantitative reverse transcription polymerase chain reaction (RT-PCR) were assessed and performed, respectively, as described in Ostendorf *et al.* [19]. Real-time RT-PCR were normalized using eukaryotic 18S ribosomal ribonucleic acid (rRNA) using the Comparative CT-method (CT) method. Primers (FAM^{TM} dye-labelled probes from ThermoFisher Scientific): VEGF-A (Mm00437306_m1, which exclude genomic DNA contaminants) and 18S rRNA (Hs99999901_s1).

For perfusion fixation, mice were anaesthetized and kidney(s) were perfused via the left ventricle with 3% paraformaldehyde in PBS (pH 7.6) for 3 min. Pieces of the kidney(s) were snap-frozen in liquid nitrogen or (post-)fixed in 3% buffered formalin and embedded in paraffin. 'Immunofluorescence' stainings were performed on 2-µm paraffin sections using primary antibodies anti-PV-1 (MECA32) (1:100, sc-19603 Santa Cruz Biotechnology, Dallas, TX, USA) and synaptopodin (1:100, sc-21537 Santa Cruz Biotechnology). Donkey anti-rabbit, -mouse or -rat Dylight 488 or Dylight 549 (1:200, Dianova, Hamburg, Germany) served as secondary antibodies. When staining mouse sections, secondary antibodies were adsorbed with 4% normal mouse serum. Nuclei were stained using Hoechst 33342 (Sigma Aldrich, St Louis, MO, USA). Sections were evaluated with a Keyence BZ-9000 microscope using BZ-II Analyzing software (Keyence Corporation, Osaka, Japan).

For 'immunohistochemistry', paraffin sections were blocked with avidin/biotin blocking kit (Vector Laboratories, Burlingame, CA, USA) and 3% H_2O_2. The sections were subjected to microwave antigen retrieval in Antigen Unmasking Solution (Vector Laboratories) followed by incubation with antibodies (secondary: biotinylated goat anti-rabbit, Vector Laboratories). Detection was carried out with vectorstain ABC kit (Vector Laboratories) using peroxidase as label and 3-amino-9-ethylcarbazole as substrate.

For transmission electron microscopy (TEM), tissue was fixed with 2% paraformaldehyde and 2.5% glutaraldehyde in 0.1 M sodium cacodylate buffer and processed for TEM.

VEGF enzyme linked immunosorbent assay (ELISA) (mVEGF-A, R&D, Minneapolis, MN, USA) was used.

For deglycosalation and immunoblot analysis, recombinant human $VEGF_{121}$ or $VEGF_{165}$ (Symansis, Temecula California, USA) was denatured at 85°C or 50°C and deglycosylated using the Glycoprotein Deglycosilation Kit (Calbiochem, Merck, Darmstadt, Germany). Afterwards the proteins were loaded with Laemmli on NuPAGE 4-12% Bis Tris Zoom Gels (Invitrogen, Carlsbad, CA, USA) for sodium dodecyl sulfate polyacrylamide gel electrophoresis (SDS-PAGE). After gel electrophoresis, the proteins were transferred on nitrocellulose membranes (Protan, Whatman, Dassel, Germany) followed by a reversible staining with PonceauS (Sigma-Aldrich, St. Louis, MI, USA) to control transfer efficiency and compare protein loading. For immunodetection, the membrane was blocked in RotiBlock (Carl Roth, Karlsruhe, Germany) and incubated using goat polyclonal anti-human VEGF antibody (R&D Systems, Minneaplis, USA) followed by a horseradish peroxidase (HRP)-conjugated secondary antibody (anti-goat; Dako Agilent, Santa Clara, CA, USA). Signals were visualized by enhanced chemiluminescence (ECL) or Super Signal Femto (Pierce Protein Biology, Thermo Scientific, Waltham, MA, USA) and digitally detected by LAS- 3000 (Fujifilm, Minato, Tokio, Japan).

For two-dimensional gel electrophoresis, proteins were separated in the first dimension by isoelectric focussing using the Ettan IGPhor 3 IEF System and Immobiline DryStrips pH 3-10 (GE Healthcare, Uppsala, Sweden) and in the second dimension by SDS-PAGE in NuPAGE 4–12% Bis-Tris ZOOM Gels

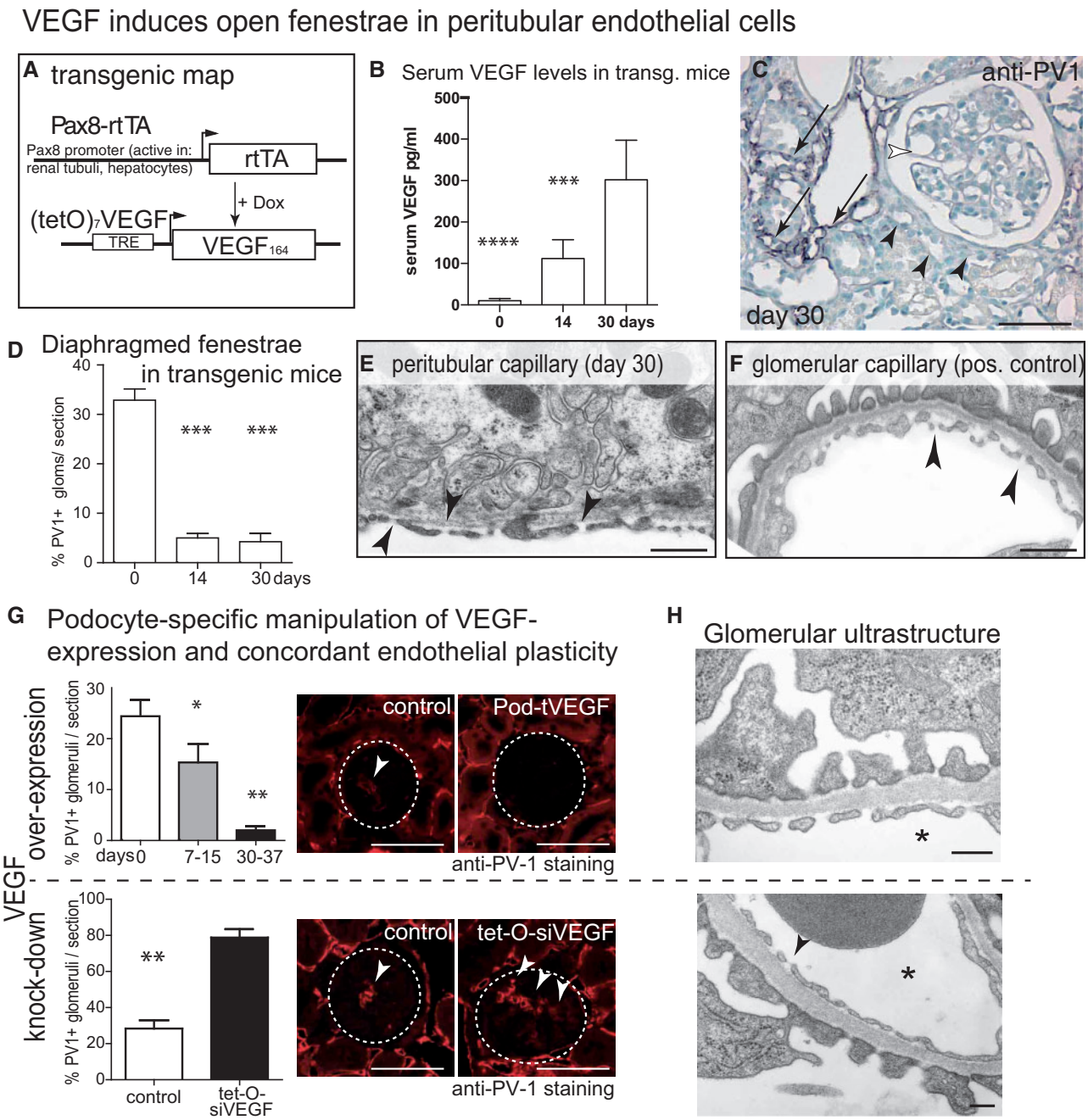

FIGURE 1: VEGF induces open fenestrae in peritubular endothelial cells**.** (**A**) Transgenic map of systemic inducible VEGF overexpression in Pax8-rtTA-VEGF$_{164}$ mice. (**B**) Serum VEGF levels in Pax8-rtTA-VEGF$_{164}$ mice. (**C**) Immunostaining for diaphragmed fenestrae (PV-1) in VEGF-overexpressing transgenic mice showed partial preservation (arrows) or absence of diaphragmed endothelia within the tubulo-interstitium (black arrowheads). Within the glomeruli, hypertrophy and complete absence of PV-1 staining was noted (white arrowhead). (**D**) On random glomerular cross-sections, the fraction of glomeruli with PV-1-positive (i.e. diaphragmed) endothelial fenestrations was reduced significantly after induction of VEGF overexpression (50 glomeruli from 7 different animals per time point, one-way ANOVA, Bonferroni *post hoc* test; ***$P < 0.001$). (**E–F**) On TEM, tubular endothelial cells formed open fenestrae in VEGF-overexpressing mice (arrowheads). Manipulating VEGF expression in podocytes results in concordant changes of endothelial morphology. (**G**) VEGF overexpression in podocytes of transgenic Pod-rtTA/(TetO)$_7$-VEGF$_{164}$ abolished formation of diaphragmed fenestrae in endothelial cells ($n = 5$ per time point). In the opposite experiment, partial knock-down of endogenous VEGF in inducible Pod-rtTA/(TetO)$_7$-siVEGF mice after 7 days [16], showed significant upregulation of diaphragmed fenestrae. Semi-quantitative evaluation of diaphragmed endothelia was performed by immunostainings for PV-1-positive glomeruli (50 glomeruli per mouse, $n = 4$ per time point, one-way ANOVA, Bonferroni *post hoc* test, *$P < 0.05$; **$P < 0.01$; ***$P < 0.001$; ****$P < 0.0001$), dashed circles mark representative glomeruli; arrows, PV-1 staining). (**H**) TEM showed no signs of endotheliosis in both transgenic mouse models (arrowheads; asterisks mark capillary lumen). Scale bars 50 µm for light microscopy, 0.5 µm for TEM.

(Invitrogen, Carlsbad, CA, USA) followed by immunoblotting and immunodetection as described above.

Statistical and mathematical analyses data are presented as mean ± standard error of mean (SEM) unless otherwise specified. Statistical analyses were performed using Prism software (GraphPad Software, La Jolla, CA, USA). Differences between two mean values were evaluated by Student's *t*-test. For comparison of paired right and left kidney after a uninephrectomy, the paired Student's *t*-test was used. Multiple groups were compared by one-way analysis of variance (ANOVA) with Bonferroni *post hoc* analysis. A P-value of <0.05 was considered significant. All quantitative or semi-quantitative analyses were performed in a blinded fashion (samples were blinded by a different investigator).

Mathematical modelling of VEGF transport

For mathematical estimations for VEGF back-filtration, the governing equation for VEGF concentrations across the renal filter follows from Hausmann *et al.* [20], where we adjusted the boundary conditions to the back-filtration setting (for a detailed summary, see Supplementary data). We thus obtained a first-order linear ordinary differential equation with constant coefficients, which can be solved analytically. To facilitate parameters studies, a Graphical User Interface was set up in MATLAB®, which allowed the user to adjust the various parameters entering the model (e.g. electric field, charge, pore size).

RESULTS

Glomerular endothelial plasticity as surrogate marker for local VEGF levels

Endogenous local VEGF levels are difficult to determine precisely *in vivo*. However, endothelial fenestrations have been described as surrogate marker for local VEGF bioactivity—in peripheral as well as glomerular capillaries (Supplementary data, Figure S1B) [21–25]. Increasing VEGF levels are associated with a transition from a continuous endothelium without fenestrae to fenestrae with diaphragms. In the present study, this tool was utilized and further developed in order to detect higher VEGF levels (Supplementary data, Figure S1B, marked in red). Glomerular capillaries of the kidney are unique in that the endothelial cells form fenestrae without diaphragms (i.e. open fenestrae, Supplementary data, Figure S1B) [26]. Here, we report three experimental findings supporting the notion that higher levels of back-filtered VEGF are sufficient to mediate this unique endothelial phenotype.

Systemic VEGF overexpression induces open fenestrae in endothelial cells in- and outside the renal glomerulus

In transgenic Pax8-rtTA/$(TetO)_7$-$VEGF_{164}$ mice, murine $VEGF_{164}$ was overexpressed in an inducible fashion in tubular epithelial cells of the kidney (Figure 1A–F). As reported previously [14], increased VEGF levels were sufficient to induce open fenestrae in peritubular endothelial cells outside of the glomerulus (Figure 1C). For semi-quantitative analysis, endothelial diaphragms were detected by immunostaining for 'plasmalemmal vesical-associated protein 1' (PV-1) [27, 28] (Figure 1C). To exclude endotheliosis, the findings were confirmed by TEM, where peritubular capillaries formed open fenestrae identical to glomerular endothelial cells (Figure 1E and F). The use of an inducible transgenic mouse model to overexpress VEGF demonstrated that open fenestrae can be induced in adult mice (excluding a developmental phenotype).

In our Pax8-rtTA/$(TetO)_7$-$VEGF_{164}$ mouse model, serum VEGF levels were increased. Therefore, glomerular capillaries were exposed to increased levels of VEGF via the systemic blood circulation (Figure 1B) [14]. Upon induction of VEGF transgene expression, the frequency of glomeruli containing endothelial cells with diaphragmed fenestrae decreased significantly (Figure 1D). However, endothelial cells formed open fenestrae instead, consistent with the model of VEGF-dependent endothelial plasticity for higher VEGF levels (Supplementary data, Figure S1B). Endotheliosis was ruled out by TEM (Figure 1E and F) and absence of proteinuria [14].

Podocyte-specific overexpression of VEGF induces open fenestrae in glomerular endothelial cells

Next, double transgenic Pod-rtTA/$(TetO)_7$-$VEGF_{164}$ mice were analysed, in which inducible local VEGF overexpression in podocytes induced glomerular hypertrophy (Figure 1G) [13]. As shown in Figure 1G, local VEGF overexpression led to glomeruli with significantly more open endothelial fenestrae (Figure 1G). This finding supports the notion that that VEGF produced by podocytes influences glomerular endothelial cells.

In the third experiment, VEGF expression was reduced by $>50\%$ in podocytes using the inducible Pod-rtTA/$(TetO)_7$-siVEGF mouse model (Figure 1G, lower panel) [16]. Glomerular endothelial cells formed significantly more diaphragmed fenestrae within 7 days after induction of VEGF knock-down (Figure 1G). No endotheliosis was observed by TEM (Figure 1H).

Collectively, these results support the notion that endothelial morphology reflects changes in local VEGF levels also at higher concentrations *in vivo* and also in the glomerulus of the kidney. Manipulating VEGF expression specifically in podocytes leads to concordant changes of glomerular endothelial cell morphology, suggesting that podocytic VEGF is transported across the glomerular filtration barrier against the bulk current of the glomerular filtrate (VEGF back-filtration).

GFR and endothelial morphology: interruption of filtration via electrocoagulation

Next, we investigated whether manipulation of SNGFR correlates with glomerular VEGF back-filtration. Glomerular filtration was interrupted by localized electrocoagulation of the kidney cortex in adult mice, as described previously [29]. Upon application of five electrical impulses, a fraction of the tubules were ablated and filtration was interrupted in remnant atubular glomeruli (Figure 2A and B). As a consequence, progressive and global PV-1 expression as surrogate marker for formation of diaphragmed fenestrae was observed in atubular glomeruli up to 30 days after coagulation (Figure 2B–E). In the early phase of the model, it could not be determined histologically whether a glomerulus was atubular or not. In order to exclude selection

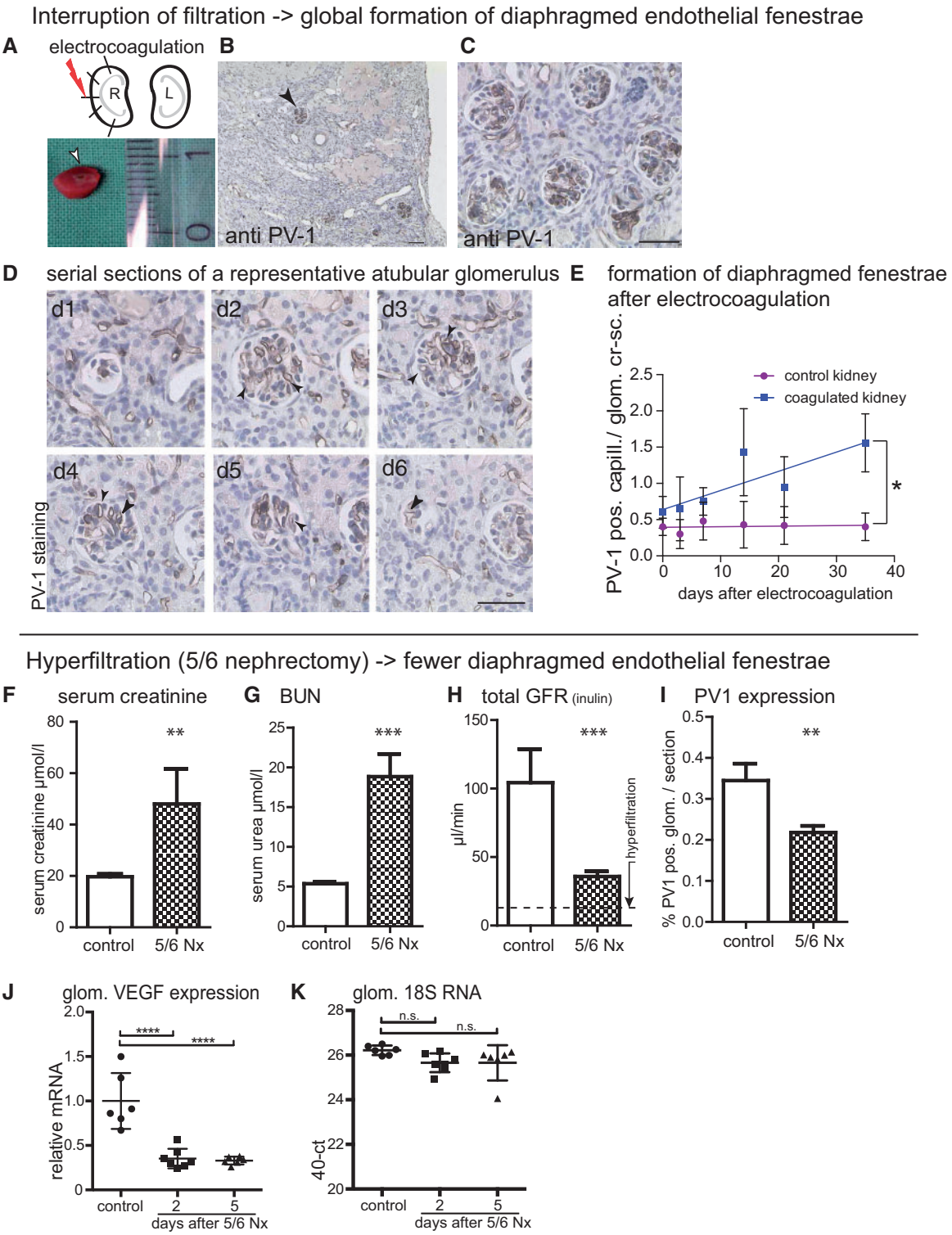

FIGURE 2: SNGFR and endothelial fenestrations. (**A–C**) Interruption of filtration-induced formation of diaphragmed fenestrae. The cortex of the right kidney was subjected to five electrocoagulations resulting in focal disruption of tubuli and tubulo-interstitial fibrosis. Arrow head, PV-1-positive glomerular cross-section. (**D**) Atubular glomeruli (verified by serial sectioning) are perfused but can no longer filter, and show global *de novo* expression of PV-1 (dark staining, arrow heads). (**E**) Formation of diaphragmed fenestrae (i.e. PV-1-positive capillary cross-sections per glomerular cross-sections) occurred over a period of 35 days ($n = 2$ mice per time point; slopes significantly different in a linear regression analysis, *P = 0.0197). Scale bars in (**D**), 50 µm; in (**B**, **C**) 100 µm. (**F–K**) To induce hyperfiltration, subtotal nephrectomy (5/6 Nx) was performed in Bl6 mice. (F–H) Serum creatinine and BUN measurements showed increase after 5/6 Nx. Kidneys were analysed after 5 days ($n = 7$). FITC-inulin clearance decreased from 104 ± 24 µL/min in controls to 36 ± 4 µL/min (***P = 0.012) in the 5/6 Nx animals, confirming induction of hyperfiltration. (I) PV-1-positive capillary cross-sections were decreased significantly in the remnant kidneys compared to controls (Student's *t*-test; **P < 0.01). (G, J, K) Total VEGF mRNA expression was down regulated in isolated glomeruli 2 and 5 days after 5/6 nephrectomy (5/6 Nx) as shown by semi-quantitative rtPCR (****P < 0.001). BUN: blood urea nitrogen.

bias in our statistical analysis (Figure 2E), PV-1 expression was evaluated in all glomeruli (including atubular and a larger fraction of intact glomeruli) on random sections. Increased PV-1 expression suggested less VEGF back-filtration in atubular glomeruli.

In addition, PV-1 expression was analysed in incidental human atubular glomeruli, which occur preferentially in chronically injured human kidneys [29]. As shown in Supplementary data, Figure S2, ubiqitous PV-1 expression was observed in atubular glomeruli also in human kidneys.

Increased SNGFR correlates with higher vegf activity

In order to achieve glomerular hyperfiltration, C57/Bl6 mice were subjected to 5/6 nephrectomy and analysed 2 or 5 days after the operation. Glomerulosclerosis was ruled out on Periodic acid-Schiff (PAS) sections (not shown). Renal insufficiency was achieved as indicated by elevated creatinine and urea (Figure 2F and G). SNGFR was approximately doubled when considering that approximately one-sixth (i.e. 16%, indicated by dashed line in Figure 2H) of remnant renal mass generated 30% of the initial GFR. Under these conditions, glomerular endothelial cells formed significantly fewer diaphragmed fenestrae (Figure 2I).

Increased glomerular VEGF expression may be a possible explanation for these results. However, VEGF-A mRNA levels were found to be down-regulated in isolated glomeruli after 5/6 nephrectomy (Figure 2J and K) arguing against increased VEGF expression as major contributor to the apparent increase in VEGF back-filtration in hyperfiltration.

Endothelial morphology in pax8-cre/beta-catenin$^{fl/fl}$ Knock-out Mice

Pax8-Cre/beta-catenin$^{fl/fl}$ knock-out mice (Figure 3A) show a developmental defect in ~10% of the glomeruli, whereby the inner aspect of Bowman's capsule is lined by fully differentiated podocytes (termed parietal podocytes) instead of parietal epithelial cells (Figure 3B–D) [17]. The parietal podocytes were shown to express similar amounts of VEGF as visceral podocytes, recruited periglomerular capillaries and formed a morphologically almost normal filtration barrier [17]. Thus, the mouse model forms two filtration barriers within the same glomerulus: periglomerular capillaries which arise from peritubular capillaries, which have low effective filtration pressures ($P_{periglom\ capillary} - P_{Bowman's\ space} \approx$ near zero) (Figure 3D). On the other hand, the high-pressure capillaries of the glomerular tuft filter normally (as indicated by the lack of proteinuria in these mice) [17]. As shown by TEM, both filtration barriers are similar (both form a GBM-like basement membrane) (Figure 3D–E'). As shown in Figure 3B–B' and C–C', endothelial cells formed diaphragmed fenestrae in periglomerular (low-pressure) capillaries consistent with lower VEGF back-filtration. Endothelial cells of high-pressure capillaries formed open fenestrae within the same glomerulus indicating higher VEGF back-filtration. In summary, the experiments described above suggest a correlation of SNGFR to VEGF back-filtration. These data support the hypothesis that increased SNGFR results in increased VEGF back-filtration and vice versa.

Endothelial PV-1 expression along the glomerular capillary

A specific sequence of morphological changes has been described previously in 1991 by Elger *et al.* [30] in glomerular endothelial cells along the length of glomerular capillaries (Supplementary data, Figure S3A and B): first, at the afferent arteriole, glomerular endothelial cells form open fenestrae. Towards the efferent arteriole, fenestrae become diaphragmed. Finally, endothelial cells are continuous and capillary filtration no longer occurs. This sequence of endothelial changes suggests decreasing VEGF back-filtration along the length of the glomerular capillaries. Indeed, effective filtration pressures and flux decrease towards the efferent arteriole due to increasing oncotic pressures (termed filtration pressure reduction or even equilibrium) (Supplementary data, Figure S3C).

To investigate this relationship further, capillary sealing was analysed in mice where subcortical superficial glomeruli are significantly smaller than juxtamedullary glomeruli. Since all filtering glomerular capillaries are known to be arranged in parallel [31] (Figure 4A), the glomerular capillaries of the superficial glomeruli are shorter compared to those of the larger juxtamedullary glomeruli. When examining the microanatomical location of diaphragmed fenestrae within small superficial glomeruli, PV-1 expression was restricted to the immediate proximity of the efferent arteriole (Figure 4B). This finding is consistent with the notion that filtration pressure reduction (or equilibrium) occurred at the end of the glomerular capillaries. As shown on serial sections of the larger juxtamedullary glomeruli in Figure 4C–E, endothelial cells formed diaphragmed fenestrae already within the glomerular capillary tuft. These findings suggest that capillary sealing is regulated and may depend on physiological parameters (such as effective filtration pressures). In human kidney, diaphragmed fenestrae were also detected exclusively towards the efferent arteriole (Figure 4F).

Mathematical modelling of VEGF back-filtration

The above-described experimental findings demonstrate a proportional relationship between effective SNGFR and effective filtration pressures and VEGF back-filtration. In order to test for potential mechanisms, the individual fluxes of VEGF against the bulk flow of the filtrate across the filter were analysed using our previously described mathematical model of glomerular filtration to simulate two models of glomerular filtration [20] (Figure 5 and Supplementary data).

In the pore model [32, 33], the glomerular filter is regarded as an impermeable membrane perforated by highly defined small pores, which allow the passage of small solutes (e.g. water, salt; blue arrows in Figure 5A). Albumin is driven into the filter by convection and diffusion; and repelled by size exclusion (black arrow). Small amounts of albumin may pass through rare 'large pores', which are specific for albumin (dashed arrow). As shown in Figure 5C, VEGF back-filtration is driven by diffusion alone in this model. Thus, VEGF back-filtration is predicted to be reduced or virtually constant when GFR is increased. Therefore, this model of glomerular filtration did not predict the results for our experimental findings.

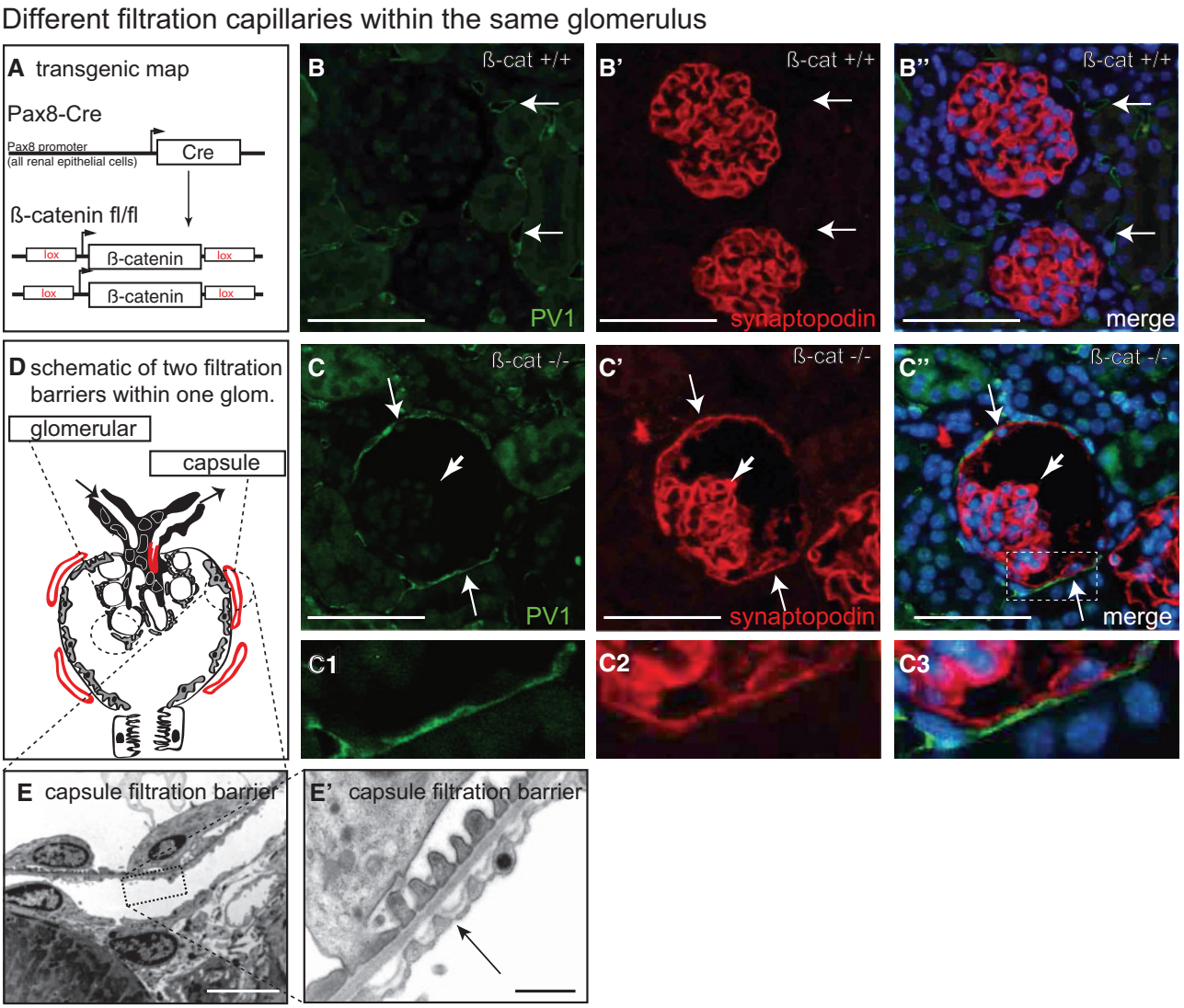

FIGURE 3: Glomerular and parietal filtration barrier within the same glomerulus. (**A**) Transgenic map of experimental animals. (**B**) In control mice, PV-1-positive can be detected in peritubular capillaries (arrows). No podocyte marker can be detected on Bowman's capsule. (**C–C"**) In beta-catenin knock-out mice [17], the Bowman's capsule is lined by parietal podocytes as shown by synaptopodin co-staining (arrows in C'). The glomerulus filters primary filtrate into a morphologically normal tubular system [17]. (**C1–C3**) In beta-catenin knock-out mice, parietal podocytes are fully differentiated (synaptopodin-positive cells, arrows), recruit peritubular capillaries and form a morphologically normal filtration barrier (higher magnification in panels B–B") (scale bars 75 µm). In the TEM in C–C' the arrows indicate fenestrae of endothelial cells with diaphragms. Endothelial cells within periglomerular capillaries formed fenestrae with diaphragms (panels C–C", arrow, C1–3, E–E') ($n = 5$ per group). Scale bars 2 µm in E, 0, 5 µm in E'.

The electrokinetic model is an expansion of the pore model, which considers also electrical effects [20, 29, 34–38]. According to this model, glomerular filtration works in two steps, which occur simultaneously (Figure 5B). First, forced filtration generates an electrical field across the glomerular filter (streaming potential), which is proportional to filtration pressures (and SNGFR). Secondly, negatively charged plasma proteins are repelled by electrophoresis (electromigration) from entering the filter (Figure 5B, black arrow in Step 2) [20, 29, 34–38]. As shown in Figure 5C, the electrokinetic model predicts a proportional increase in VEGF back-filtration with increasing GFR. The model suggests electrical effects as a candidate force to drive VEGF across the filter against the bulk flow of the filtrate.

The above-described outside-in electrophoretic transport of VEGF can occur only if the mobile isoforms of VEGF are negatively charged. To test this, the electrostatic charge of human isoforms of recombinant VEGF was determined experimentally. Since glycosylation modifies the electrostatic charge significantly, recombinant VEGF expressed in eukaryotic cells was used assuming that the glycosylation pattern is most similar to the situation *in vivo*. Recombinant murine VEGF expressed in eukaryotic cells was not available at the time of the study.

As shown in Figure 6A, the mobile $hVEGF_{110\text{-}113}$ and $hVEGF_{121}$ isoforms share a common anionic N-terminus and lack the cationic C-terminus of the longer isoforms ($VEGF_{165}$ and $VEGF_{189}$). Biologically active $VEGF_{110\text{-}113}$ can be generated

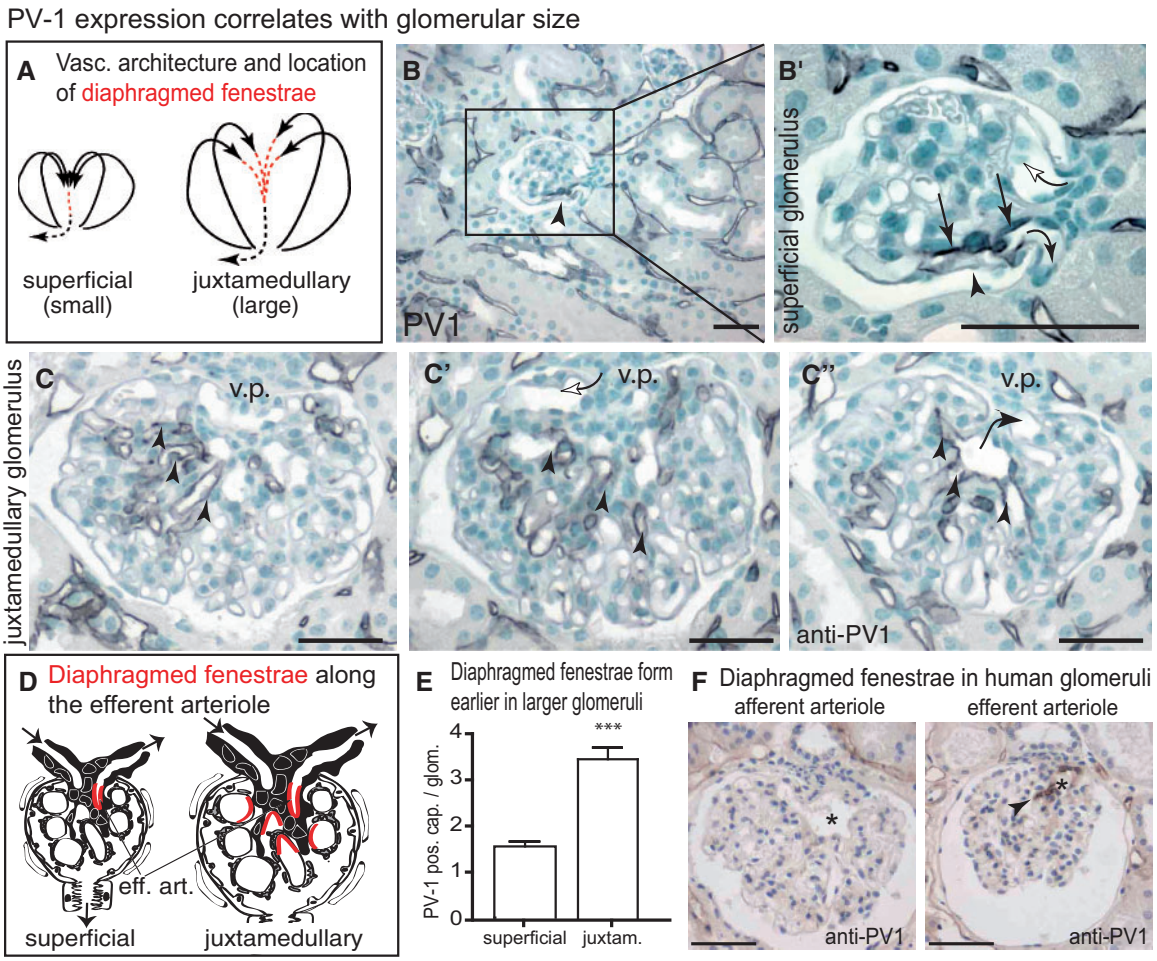

FIGURE 4: Capillary microvasculature of the glomerulus. (**A**) The afferent arteriole branches immediately into multiple paralell filtering capillaries [31]. The location of endothelial cells with diaphragmed fenestrae is marked in red, continuous endothelial cells are marked as black dotted line. (**B, B'**) In superficial glomeruli, endothelial cells with diaphragmed fenestrae localized exclusively towards the efferent arteriole (arrows, anti-PV-1 staining in serial sections of 10 healthy mice; arrowhead shows slightly reduced PV-1 staining towards the outer filtering aspect compared with the inner aspect of the efferent arteriole, which is predicted to filter less due to mesangial cells). The glomerular vas afferens can be identified because it branches immediately into multiple capillaries and it was always negative for PV-1 (white arrow; afferent and efferent arterioles are marked). (**C–C"**) When analysing the larger juxtamedullary glomeruli on serial sections, more intraglomerular capillary cross-sections formed diaphragmed PV-1-positive fenestrae. Positive cross-sections occurred earlier within the tributaries of the efferent arteriole (arrow in C") and were often located already within the capillary tuft (arrowheads). v.p., vascular pole. (**D**) Schematic of the microanatomical location of diaphragmed fenestrae (in red) within the smaller superficial and larger juxtamedullary glomeruli. (**E**) Statistical analysis of the frequency of PV-1-positive capillary cross-sections per random glomerular cross-section in superficial versus juxtamedullary cross-sections (50 superficial or juxtamedullary glomeruli from 6 female Sv129 mice, respectively; Student's *t*-test, *** $P < 0.001$). (**F**) In normal human kidney, no PV-1 expression was detected in the vas afferens (asterisk). In contrast, the vas efferens stained positive (arrow head), confirming our findings in rodents. Scale bars 50 μm.

by proteolytic cleavage of the C-terminus by plasmin, urokinase, and metalloproteases from any of the larger VEGF isoforms [39–42]. All of these proteases are expressed within the renal glomerulus [43–46]. *In vitro* digestions indicated that the human $VEGF_{121}$ isoform is not glycosylated, whereas the $VEGF_{165}$ isoform is glycosylated—most likely within the additional C-terminal 44 amino acids (Figure 6B–D'). Assuming that the highly similar murine $VEGF_{120}$ isoform is also not glycosylated, the overall charge of the VEGF mobile isoforms can be calculated from sequence analysis alone: the predicted charge of $VEGF_{110\text{-}113}$ is −10; and of $VEGF_{121}$ is −4. The negative charge of $VEGF_{120}$ was confirmed experimentally by 2D gel electrophoresis (Figure 6C and C'). In summary, our experiments confirmed that the mobile isoforms of recombinant human VEGF are negatively charged.

DISCUSSION

In the present study, the model of endothelial morphology was extended and validated to detect also higher levels of VEGF. The results of the present study show that VEGF backfiltration is regulated and correlates with SNGFR *in vivo*. Mathematical modelling of VEGF fluxes according to two models of glomerular filtration revealed that in addition to diffusion, streaming potentials generated by filtration could be a potential candidate force to drive VEGF against the bulk flow of the filtrate across the filter by electrophoresis.

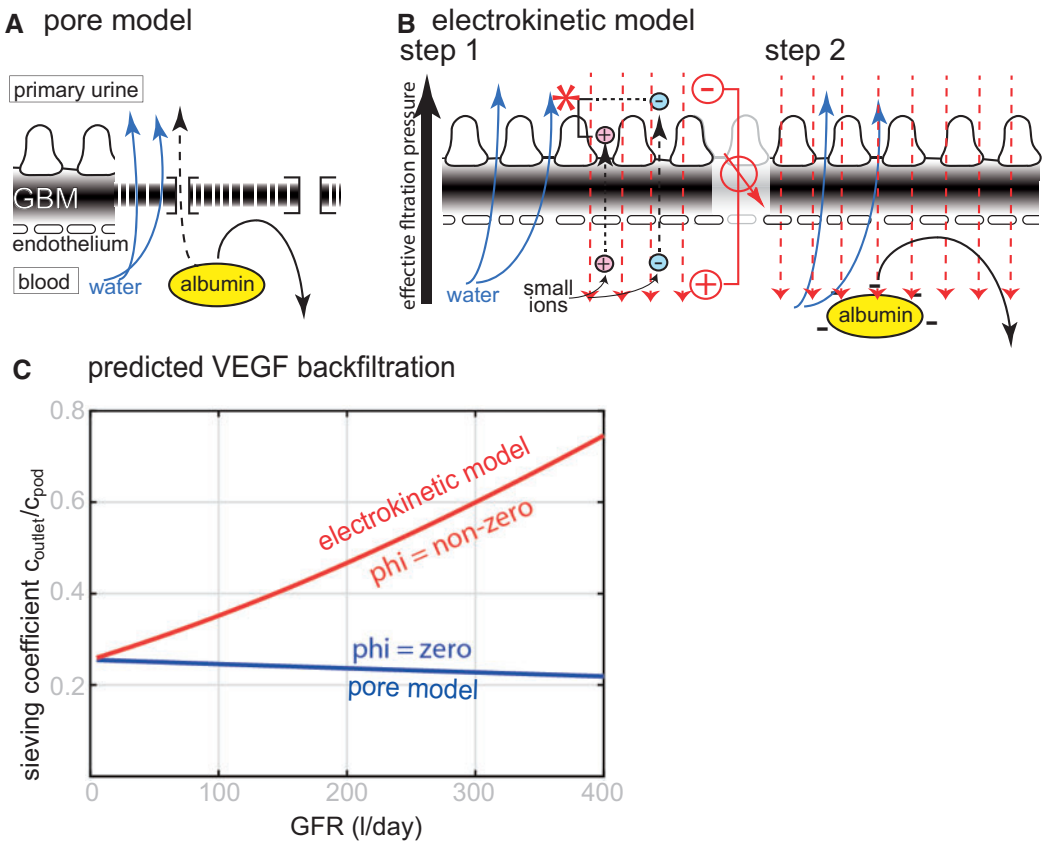

FIGURE 5: Predicted mechanisms driving VEGF back-filtration in the pore model or electrokinetic model. (**A**) In the pore model, the glomerular filter is regarded as impermeable membrane perforated by small and large pores with defined diameter. (**B**) In the electrokinetic model, a streaming potential (red) is generated by forced filtration of the small ions (Step 1). First, forced filtration of the small ionic molecules (water; blue arrows, and small ions, i.e. salts; dashed black arrows) across the charged filter generates an electrical field, called streaming potential (red). It is generated because the small positively charged cations (e.g. sodium, potassium; red ions) pass the filter slightly slower than negatively charged anions (e.g. chloride, bicarbonate; blue ions), generating the zeta potential (red asterisk) which is proportional to GFR. In Step 2, which occurs simultaneously, negatively charged plasma proteins are pushed back by electrophoresis by the streaming potential. (**C**) In both models of glomerular filtration, total VEGF back-filtration was analysed mathematically depending on GFR (here shown as sieving coefficient of the total amount of released VEGF from podocytes at the outside of the filter). The calculations predict decreasing VEGF concentrations at the end of the glomerular capillary in the pore model versus increasing VEGF concentrations in the electrokinetic model.

Potential factors influencing regulated vegf back-filtration

It is unlikely that differential expression of VEGF in podocytes mediated the observed correlation between SNGFR and endothelial morphology. We show that global expression of VEGF was decreased in hyperfiltration, therefore it cannot explain the observed apparent increase in VEGF back-filtration (Figure 2J and K). Our findings are also consistent with published reports of glomerulomegaly in cyanotic heart diseases in humans or in mice after podocyte-specific inactivation of von-Hippel-Lindau (VHL) [47, 48], where VEGF synthesis is increased in podocytes.

Differential release of VEGF from individual podocytes is also an unlikely explanation for the observed decreasing VEGF activity towards the efferent arteriole because podocytes usually cover several capillaries and thus overlap significantly with multiple other podocytes. Finally, there is exquisite gene dosage sensitivity of VEGF, e.g. development of focal segmental glomerulosclerosis (FSGS) upon inactivation of one VEGF allele in podocytes. As outlined by Eremina *et al.* [49], this argues against a potential regulatory mechanism to adjust VEGF expression levels in podocytes to mediate the observed effects in this study [49].

Electrophoretic transport as candidate mechanism coupling sngfr to vegf back-filtration

Mathematical modelling suggested that electrical effects may drive VEGF back across the glomerular filter. The electrical field is generated by a streaming potential which has been directly measured in micropuncture experiments [20]. It is directly proportional to SNGFR and negative in Bowman's space (Figure 5B). The specific polarity of the streaming potential in the glomerulus has been detected also in a general diffusion porin channel of *Escherichia coli* and *ex vivo* across the bovine lense basement membrane (which is similar to the glomerular basement membrane (GBM)) [50, 51].

Electrophoretic back-filtration of VEGF is consistent with all of our experimental findings. In atubular glomeruli, where filtration was interrupted acutely, we found that VEGF back-filtration was decreased even though one would expect the opposite. If the convective outward flow of the primary filtrate is

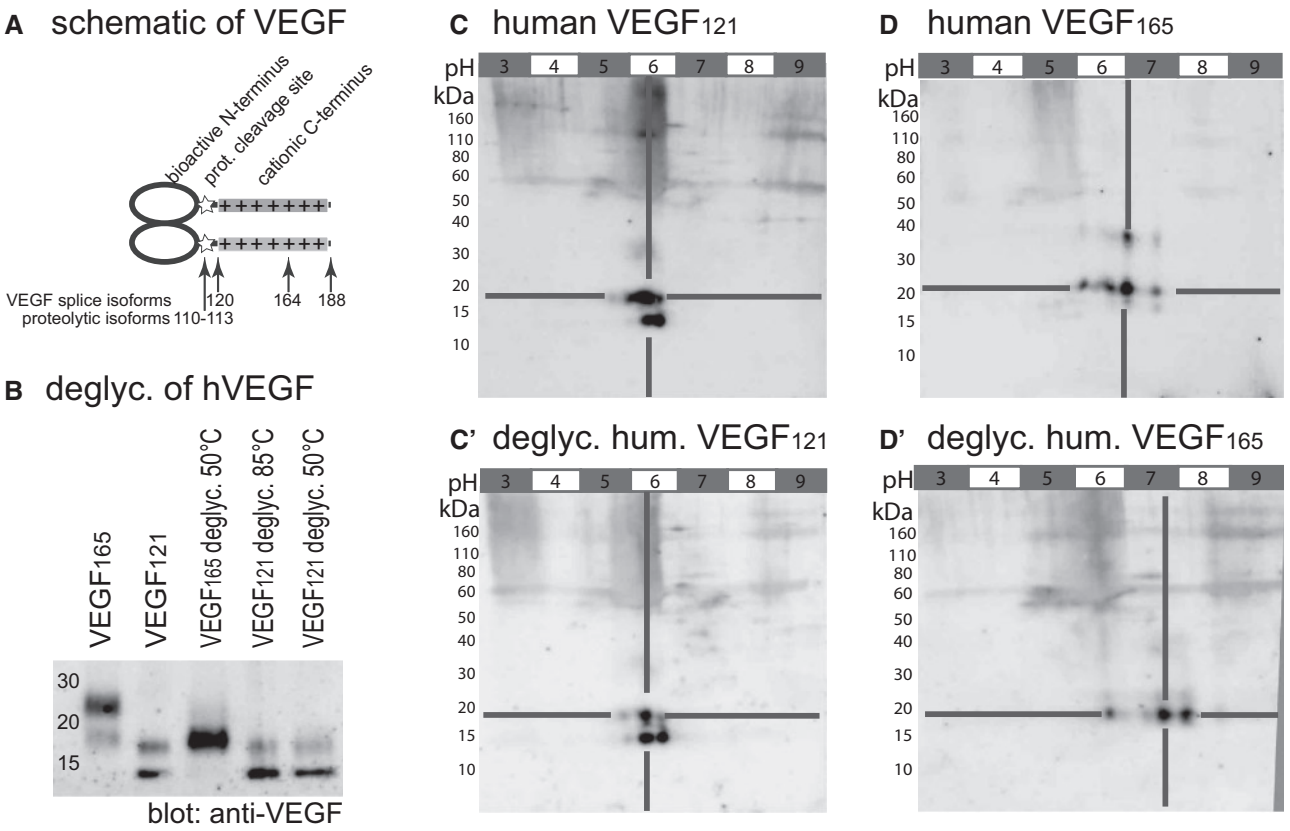

FIGURE 6: Electrostatic charge of VEGF isoforms. (**A**) Schematic of the VEGF-A molecule. The N-terminal 110 amino acids of VEGF form a homodimer and bind and activate VEGF receptors. The C-terminus ($VEGF_{120\text{-}188}$) is positively charged and immobilizes VEGF to cell surfaces and extracellular matrix. The N-terminus is separated from the cationic C-terminus by multiple proteolytic cleavage sites (asterisk) at positions 110–118. (**B**) SDS-PAGE and subsequent immunoblot of recombinant human VEGF isoforms 121 and 165 expressed in eukaryotic cells. Deglycosylation modifies the apparent molecular weight of $hVEGF_{165}$; $VEGF_{121}$ remains unaffected. (**C–D'**) To evaluate whether glycosylation modifies the charge of VEGF isoforms, 2D gel electrophoresis (isoelectric focussing/SDS-PAGE) was performed before and after deglycosylation. (C, C') Human $VEGF_{121}$ had an apparent molecular weight of ∼15 and ∼18 kDa. Deglycosylation of O- and N-linked oligosaccharides did not affect the anionic charge of the protein (pI ∼6). (D, D') Human $VEGF_{165}$ showed an apparent molecular weight of ∼20 and ∼50 kDa, deglycosylation resulted in a slightly smaller and more cationic protein (pI ∼6, 5 → 7, 5) (B–D'; representative immunoblots of at least three independent experiments, each). In summary, glycosylation was detected in the C-terminal 44 amino acids of $hVEGF_{165}$ (A) but not in $hVEGF_{121}$ (B–D'). Sequence analysis predicts a calculated negative (anionic) charge of $z = -4$ or -10 for homodimers of $VEGF_{120}$ or proteolytically cleaved $VEGF_{110\text{-}113}$, respectively.

abolished by coagulating the tubule, VEGF should be accumulating in Bowman's space and higher amounts of VEGF should be diffusing across the filter.

The biophysical phenomenon of streaming potentials *in vivo* is a relatively recent and novel discovery. This is the first report, proposing that the activity of a secreted growth factor (VEGF) is additionally regulated by extracellular streaming potentials.

VEGF as model growth factor system

This study focussed on growth factor VEGF as a model growth factor system. Within the glomerulus, a crucial and essential functional role is well established for VEGF, where it mediates several important effects, including glomerular size. It is very likely that VEGF is not the only factor regulating endothelial cell fenestrations and glomerular size. Glomerular cells secrete several growth factors (e.g. angiopoietins, bone morphogenic proteins, platelet-derived growth factors [52, 53]) and their activity is regulated by multiple mechanisms (expression levels, proteolytic cleavage). Other additional effects including haemodynamic effects (e.g. shear forces) or other direct effects on endothelial cells may also play a role. Another major limitation of this study is that VEGF levels can only be measured indirectly using the established model of endothelial morphology as surrogate marker [21–25]. To consider or compensate other known and unknown potential effects, significant efforts were undertaken to employ different *in vivo* models in the present study.

SUPPLEMENTARY DATA

Supplementary data are available at ndt online.

FUNDING

M.J.M. is a Heisenberg fellow by the Deutsche Forschungsgemeinschaft (DFG) (DFG MO 1082/7-1). This work was supported by the consortium STOP-FSGS by the German Ministry for Science and Education (BMBF 01GM1518A to M.J.M.), and TP04, TP17, Q2 SFB/Transregio

57 of the DFG (to C.T. and M.J.M.) and a Boost Fund OPBo45 of the Excellence Initiative by the German Federal and State Governments (DFG to M.G., R.H. and M.J.M.). C.K., T.S. and S.K.S. were supported by a START grant and C.K. and T.S. by a *Rotationsstellen* programme of the Faculty of Medicine of the RWTH Aachen University and by a grant of the Else-Kröner-Fresenius Foundation (A200/2013 to C.K. and 2015/A197 to T.S.). Additional support came from the Interdisciplinary Center for Clinical Research (IZKF) Aachen within the Faculty of Medicine of RWTH Aachen University. A.T. was supported by NIH grants RO1-DK59333 and P30-DK-07910 (George M.O'Brien Kidney Center at Yale). M.J.M. and J.F. are members of the SFB/Transregio 57 DFG consortium 'Mechanisms of organ fibrosis'.

CONFLICT OF INTEREST STATEMENT

None of the authors declare a competing financial interest regarding this study.

(See related article by Yamaguchi and Canaud. Vascular endothelial growth factor backfiltration in the glomerulus: an intriguing mechanism. *Nephrol Dial Transplant* 2018; 33: 1483–1484)

REFERENCES

1. Eremina V, Sood M, Haigh J *et al.* Glomerular-specific alterations of VEGF-A expression lead to distinct congenital and acquired renal diseases. *J Clin Invest* 2003; 111: 707–716
2. Sison K, Eremina V, Baelde H *et al.* Glomerular structure and function require paracrine, not autocrine, VEGF-VEGFR-2 signaling. *J Am Soc Nephrol* 2010; 21: 1691–1701
3. Jin J, Sison K, Li C *et al.* Soluble FLT1 binds lipid microdomains in podocytes to control cell morphology and glomerular barrier function. *Cell* 2012; 151: 384–399
4. Haraldsson B, Barisoni L, Quaggin SE. Reply to: VEGF inhibition and renal thrombotic microangiopathy. *N Engl J Med* 2008; 359: 205–207
5. Hayslett JP, Kashgarian M, Epstein FH. Functional correlates of compensatory renal hypertrophy. *J Clin Invest* 1968; 47: 774–799
6. Krohn AG, Peng BB, Antell HI *et al.* Compensatory renal hypertrophy: the role of immediate vascular changes in its production. *J Urol* 1970; 103: 564–568
7. Kaufman JM, Siegel NJ, Hayslett JP. Functional and hemodynamic adaptation to progressive renal ablation. *Circ Res* 1975; 36: 286–293
8. Northrup TE, Malvin RL. Cellular hypertrophy and renal function during compensatory renal growth. *Am J Physiol* 1976; 231: 1191–1195
9. Pecly IM, Genelhu V, Francischetti EA. Renal functional reserve in obesity hypertension. *Int J Clin Pract* 2006; 60: 1198–1203
10. Helal I, Fick-Brosnahan GM, Reed-Gitomer B *et al.* Glomerular hyperfiltration: definitions, mechanisms and clinical implications. *Nat Rev Nephrol* 2012; 8: 293–300
11. Tomaszewski M, Charchar FJ, Maric C *et al.* Glomerular hyperfiltration: a new marker of metabolic risk. *Kidney Int* 2007; 71: 816–821
12. Hoeben A, Landuyt B, Highley MS *et al.* Vascular endothelial growth factor and angiogenesis. *Pharmacol Rev* 2004; 56: 549–580
13. Veron D, Reidy KJ, Bertuccio C *et al.* Overexpression of VEGF-A in podocytes of adult mice causes glomerular disease. *Kidney Int* 2010; 77: 989–999
14. Hakroush S, Moeller MJ, Theilig F *et al.* Effects of increased renal tubular vascular endothelial growth factor (VEGF) on fibrosis, cyst formation, and glomerular disease. *Am J Pathol* 2009; 175: 1883–1895
15. Schrijvers BF, Flyvbjerg A, De Vriese AS. The role of vascular endothelial growth factor (VEGF) in renal pathophysiology. *Kidney Int* 2004; 65: 2003–2017
16. Veron D, Villegas G, Aggarwal PK *et al.* Acute podocyte vascular endothelial growth factor (VEGF-A) knockdown disrupts alphaVbeta3 integrin signaling in the glomerulus. *PLoS One* 2012; 7: e40589
17. Grouls S, Iglesias DM, Wentzensen N *et al.* Lineage specification of parietal epithelial cells requires beta-catenin/Wnt signaling. *J Am Soc Nephrol* 2012; 23: 63–72
18. Qi Z, Whitt I, Mehta A *et al.* Serial determination of glomerular filtration rate in conscious mice using FITC-inulin clearance. *Am J Physiol Renal Physiol* 2004; 286: F590–F596
19. Ostendorf T, van Roeyen CR, Peterson JD *et al.* A fully human monoclonal antibody (CR002) identifies PDGF-D as a novel mediator of mesangioproliferative glomerulonephritis. *J Am Soc Nephrol* 2003; 14: 2237–2247
20. Hausmann R, Kuppe C, Egger H *et al.* Electrical forces determine glomerular permeability. *J Am Soc Nephrol* 2010; 21: 2053–2058
21. Satchell SC, Braet F. Glomerular endothelial cell fenestrations: an integral component of the glomerular filtration barrier. *Am J Physiol Renal Physiol* 2009; 296: F947–F956
22. Esser S, Wolburg K, Wolburg H *et al.* Vascular endothelial growth factor induces endothelial fenestrations in vitro. *J Cell Biol* 1998; 140: 947–959
23. Lammert E, Gu G, McLaughlin M *et al.* Role of VEGF-A in vascularization of pancreatic islets. *Curr Biol* 2003; 13: 1070–1074
24. Kamba T, Tam BY, Hashizume H *et al.* VEGF-dependent plasticity of fenestrated capillaries in the normal adult microvasculature. *Am J Physiol Heart Circ Physiol* 2006; 290: H560–H576
25. Satchell SC, Tasman CH, Singh A *et al.* Conditionally immortalized human glomerular endothelial cells expressing fenestrations in response to VEGF. *Kidney Int* 2006; 69: 1633–1640
26. Ichimura K, Stan RV, Kurihara H *et al.* Glomerular endothelial cells form diaphragms during development and pathologic conditions. *J Am Soc Nephrol* 2008; 19: 1463–1471
27. Stan RV, Tkachenko E, Niesman IR. PV1 is a key structural component for the formation of the stomatal and fenestral diaphragms. *Mol Biol Cell* 2004; 15: 3615–3630
28. Tkachenko E, Tse D, Sideleva O *et al.* Caveolae, fenestrae and transendothelial channels retain PV1 on the surface of endothelial cells. *PLoS One* 2012; 7: e32655
29. Schulte K, Berger K, Boor P *et al.* Origin of parietal podocytes in atubular glomeruli mapped by lineage tracing. *J Am Soc Nephrol* 2014; 25: 129–141
30. Elger M, Sakai T, Winkler D *et al.* Structure of the outflow segment of the efferent arteriole in rat superficial glomeruli. *Contrib Nephrol* 1991; 95: 22–33
31. Winkler D, Elger M, Sakai T *et al.* Branching and confluence pattern of glomerular arterioles in the rat. *Kidney Int Suppl* 1991; 32: S2–S8
32. Rippe B, Haraldsson B. Transport of macromolecules across microvascular walls: the two-pore theory. *Physiol Rev* 1994; 74: 163–219
33. Rippe B, Oberg CM. Counterpoint: defending pore theory. *Perit Dial Int* 2015; 35: 9–13
34. Hausmann R, Grepl M, Knecht V *et al.* The glomerular filtration barrier function: new concepts. *Curr Opin Nephrol Hypertens* 2012; 21: 441–449
35. Moeller MJ, Kuppe C. Point: proposing the electrokinetic model. *Perit Dial Int* 2015; 35: 5–8
36. Moeller MJ, Tanner GA. Reply: Podocytes are key-although albumin never reaches the slit diaphragm. *Nat Rev Nephrol* 2014; 10: 180
37. Moeller MJ, Tenten V. Renal albumin filtration: alternative models to the standard physical barriers. *Nat Rev Nephrol* 2013; 9: 266–277
38. Saritas T, Kuppe C, Moeller MJ. Progress and controversies in unraveling the glomerular filtration mechanism. *Curr Opin Nephrol Hypertens* 2015; 24: 208–216
39. Houck KA, Leung DW, Rowland AM *et al.* Dual regulation of vascular endothelial growth factor bioavailability by genetic and proteolytic mechanisms. *J Biol Chem* 1992; 267: 26031–26037
40. Plouet J, Moro F, Bertagnolli S *et al.* Extracellular cleavage of the vascular endothelial growth factor 189-amino acid form by urokinase is required for its mitogenic effect. *J Biol Chem* 1997; 272: 13390–13396
41. Lee S, Jilani SM, Nikolova GV *et al.* Processing of VEGF-A by matrix metalloproteinases regulates bioavailability and vascular patterning in tumors. *J Cell Biol* 2005; 169: 681–691
42. Eming SA, Krieg T. Molecular mechanisms of VEGF-A action during tissue repair. *J Investig Dermatol Symp Proc* 2006; 11: 79–86

43. Catania JM, Chen G, Parrish AR. Role of matrix metalloproteinases in renal pathophysiologies. *Am J Physiol Renal Physiol* 2007; 292: F905–F911
44. Angles-Cano E, Rondeau E, Delarue F *et al*. Identification and cellular localization of plasminogen activators from human glomeruli. *Thromb Haemost* 1985; 54: 688–692
45. Sappino AP, Huarte J, Vassalli JD *et al*. Sites of synthesis of urokinase and tissue-type plasminogen activators in the murine kidney. *J Clin Invest* 1991; 87: 962–970
46. Wei C, El Hindi S, Li J *et al*. Circulating urokinase receptor as a cause of focal segmental glomerulosclerosis. *Nat Med* 2011; 17: 952–960
47. Brukamp K, Jim B, Moeller MJ *et al*. Hypoxia and podocyte-specific Vhlh deletion confer risk of glomerular disease. *Am J Physiol Renal Physiol* 2007; 293: F1397–F1407
48. Hida K, Wada J, Yamasaki H *et al*. Cyanotic congenital heart disease associated with glomerulomegaly and focal segmental glomerulosclerosis: remission of nephrotic syndrome with angiotensin converting enzyme inhibitor. *Nephrol Dial Transplant* 2002; 17: 144–147
49. Eremina V, Baelde HJ, Quaggin SE. Role of the VEGF–a signaling pathway in the glomerulus: evidence for crosstalk between components of the glomerular filtration barrier. *Nephron Physiol* 2007; 106: p32–37
50. Garcia-Gimenez E, Alcaraz A, Aguilella VM. Overcharging below the nanoscale: multivalent cations reverse the ion selectivity of a biological channel. *Phys Rev E* 2010; 81: 021912-1–7
51. Ferrell N, Cameron KO, Groszek JJ *et al*. Effects of pressure and electrical charge on macromolecular transport across bovine lens basement membrane. *Biophys J* 2013; 104: 1476–1484
52. Satchell SC, Mathieson PW. Angiopoietins: microvascular modulators with potential roles in glomerular pathophysiology. *J Nephrol* 2003; 16: 168–178
53. Clement LC, Avila-Casado C, Mace C *et al*. Podocyte-secreted angiopoietin-like-4 mediates proteinuria in glucocorticoid-sensitive nephrotic syndrome. *Nat Med* 2011; 17: 117–122

Received: 12.10.2017; Editorial decision: 8.2.2018

Nephrol Dial Transplant (2018) 33: 1525–1532
doi: 10.1093/ndt/gfx362
Advance Access publication 19 January 2018

Bone disease in nephropathic cystinosis is related to cystinosin-induced osteoclastic dysfunction

Debora Claramunt-Taberner[1], Sacha Flammier[2], Ségolène Gaillard[3], Pierre Cochat[1,4], Olivier Peyruchaud[2], Irma Machuca-Gayet[2,*] and Justine Bacchetta[1,2,4,*]

[1]Centre de Référence des Maladies Rénales Rares, Hôpital Femme Mère Enfant, Hospices Civils de Lyon, Bron, France, [2]INSERM, UMR 1033, Faculté de Médecine Lyon Est, Université Claude Bernard Lyon 1, Lyon, France, [3]INSERM CIC 1407, CNRS UMR 5558 and Service de Pharmacotoxicologie Clinique, Hospices Civils de Lyon, Bron, France and [4]Université de Lyon, Lyon, France

Correspondence and offprint requests to: Justine Bacchetta; E-mail: justine.bacchetta@chu-lyon.fr
*These authors contributed equally to this work.

ABSTRACT

Background. Bone impairment is a poorly described complication of nephropathic cystinosis (NC). The objectives of this study were to evaluate *in vitro* effects of cystinosin (CTNS) mutations on bone resorption and of cysteamine treatment on bone cells [namely human osteoclasts (OCs) and murine osteoblasts].

Methods. Human OCs were differentiated from peripheral blood mononuclear cells (PBMCs) of patients and healthy donors (HDs). Cells were treated with increasing doses of cysteamine in PBMCs or on mature OCs to evaluate its impact on differentiation and resorption, respectively. Similarly, cysteamine-treated osteoblasts derived from murine mesenchymal stem cells were assessed for differentiation and activity with toxicity and proliferation assays.

Results. CTNS was expressed in human OCs derived from HDs; its expression was regulated during monocyte colony-stimulating factor- and receptor activator of nuclear factor-κB-dependent osteoclastogenesis and required for efficient bone resorption. Cysteamine had no impact on osteoclastogenesis but inhibited *in vitro* HD osteoclastic resorption; however, NC OC-mediated bone resorption was impaired only at high doses. Only low concentrations of cysteamine (50 μM) stimulated osteoblastic differentiation and maturation, while this effect was no longer observed at higher concentrations (200 μM).

Conclusion. CTNS is required for proper osteoclastic activity. *In vitro* low doses of cysteamine have beneficial antiresorptive effects on healthy human-derived OCs and may partly correct the CTNS-induced osteoclastic dysfunction in patients with NC. Moreover, *in vitro* low doses of cysteamine also stimulate osteoblastic differentiation and mineralization, with an inhibitory effect at higher doses, likely explaining, at least partly, the bone toxicity observed in patients receiving high doses of cysteamine.

Keywords: bone, cysteamine, cystinosin, nephropathic cystinosis, osteoclast